

Building a Weakly Outgassing Comet from a Generalized Ohm's Law

Jan Deca*

*Laboratory for Atmospheric and Space Physics (LASP), University of Colorado Boulder, Boulder, Colorado 80303, USA
and Institute for Modeling Plasma, Atmospheres and Cosmic Dust, NASA/SSERVI, Moffet Field, California 94035, USA*

Pierre Henri

*LPC2E, CNRS, Orléans 45071, France**Laboratoire Lagrange, CNRS, Observatoire de la Côte d'Azur, Université Côte d'Azur, Nice, France*

Andrey Divin

Physics Department, St. Petersburg State University, St. Petersburg 198504, Russia

Anders Eriksson

Swedish Institute of Space Physics (IRF), Uppsala 751 21, Sweden

Marina Galand and Arnaud Beth

Department of Physics, Imperial College London, London SW7 2AZ, United Kingdom

Katharina Ostaszewski

Institute for Geophysics and Extraterrestrial Physics (IGeP), Technische Universität Braunschweig, Braunschweig 38106, Germany

Mihály Horányi

*Laboratory for Atmospheric and Space Physics (LASP), University of Colorado Boulder, Boulder, Colorado 80303, USA,
Institute for Modeling Plasma, Atmospheres and Cosmic Dust, NASA/SSERVI, Moffet Field, California 94035, USA,
and Department of Physics, University of Colorado Boulder, Boulder, Colorado 80309, USA*

(Received 8 January 2019; revised manuscript received 21 May 2019; published 1 August 2019)

When a weakly outgassing comet is sufficiently close to the Sun, the formation of an ionized coma results in solar wind mass loading and magnetic field draping around its nucleus. Using a 3D fully kinetic approach, we distill the components of a generalized Ohm's law and the effective electron equation of state directly from the self-consistently simulated electron dynamics and identify the driving physics in the various regions of the cometary plasma environment. Using the example of space plasmas, in particular multispecies cometary plasmas, we show how the description for the complex kinetic electron dynamics can be simplified through a simple effective closure, and identify where an isotropic single-electron fluid Ohm's law approximation can be used, and where it fails.

DOI: [10.1103/PhysRevLett.123.055101](https://doi.org/10.1103/PhysRevLett.123.055101)

Numerical models that seek to describe the evolution of plasma without self-consistently including the electron dynamics, such as (multi-)fluid and hybrid simulation approaches [1], need to rely on a relation that prescribes the behavior of the unresolved species. Typically a generalized Ohm's law (GOL) is assumed [2], combined with a closure relation such as a polytropic or a double adiabatic evolution [3,4]. In this Letter, we show how a GOL can unravel the hidden mysteries of multispecies plasma environments, such as the solar wind plasma interaction with a weakly outgassing comet [5–7]. We indicate where reduced plasma models can be applied, e.g., to gain more direct access to the ongoing physics and/or to decrease the needed amount of computational resources, and show the consequences of this compromise.

The Rosetta spacecraft caught up with comet 67P/Churyumov-Gerasimenko (hereafter 67P) at a heliocentric distance of 3.6 AU [8,9]. At a few hundred kilometers from the cometary nucleus, the Rosetta plasma instruments, quite unexpectedly, picked up the signatures of a plasma environment dominated by cometary matter [10,11], even though 67P had an outgassing rate of one to two orders of magnitude smaller than 1P/Halley at a similar heliocentric distance [12–15]. This meant that even at large heliocentric distances the weakly outgassing nucleus of 67P mass loads the solar wind plasma [5,6].

Various ionization processes, such as electron-impact ionization, photo-ionization, and charge exchange, contribute to the shape of the near-cometary environment [16–18]. Rosetta observed a radial dependence of the plasma density

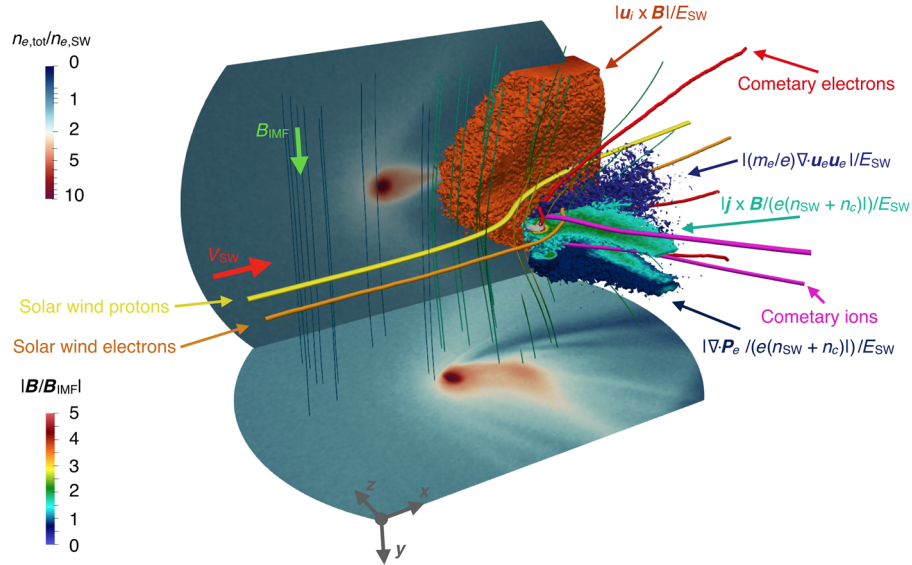


FIG. 1. Illustration of the solar wind interaction with a weakly outgassing comet representative of 67P/Churyumov-Gerasimenko at a heliocentric distance of 4.0–4.5 AU. For each simulated species, velocity streamlines representative of its dynamics are plotted. The various isovolumes represent where the respective components of the generalised Ohm’s law are significant with respect to the four-fluid behavior of the system. The projections represent the total electron density on two perpendicular planes through the center of the nucleus. Refer to Fig. 2 for exact numbers and scaling.

with distance from the nucleus [19,20] or, in other words, there exists a continuously changing ratio between the cometary and the upstream solar wind plasma density throughout 67P’s plasma environment, both along the Sun-comet direction as well as in the meridian plane [21–23]. To first order, for a weakly outgassing comet, the dynamical interaction that determines the general structure of the cometary plasma environment is representative of a four-fluid coupled system (illustrated in Fig. 1), where the solar wind electrons move to neutralize the cometary ions and the cometary electrons organize themselves to neutralize the solar wind ions [7].

In addition to a detailed understanding of the kinetic dynamics that governs the solar wind interaction with a weakly outgassing comet, in this Letter we provide feedback to (multi-)fluid [24–29] and hybrid [16,30–37] models where the electrons dynamics is prescribed through a GOL combined with an electron closure relation. Using a fully kinetic, self-consistent approach for the electron dynamics, however, we can work the other way around and compute the various terms of the GOL directly from the simulation output. Our simulation model does not assume any GOL. This allows us to identify the compromises that a simplified electron pressure tensor brings to the electron dynamics and to establish where it is justified to adopt a GOL that mimics the electron dynamics. As the locations of the solar wind and cometary species in phase space changes throughout the cometary plasma environment, so too will the balance between the different contributions to the total electric field in the GOL in response to the physical processes that dominate each region.

To simulate the solar wind interaction with comet 67P we use the semi-implicit, fully kinetic, electromagnetic particle-in-cell code iPIC3D [7,38]. The code solves the Vlasov-Maxwell system of equations for both ions and electrons using the implicit moment method [39–41]. We assume a setup identical to Deca *et al.* [7] and generate cometary water ions, and cometary electrons that result from the ionization of a radially expanding atmosphere. We adopt an outgassing rate of $Q = 10^{25} \text{ s}^{-1}$, which for 67P translates into a heliocentric distance of roughly 4.0–4.5 AU [42]. These choices are in part motivated by our desire to obtain electron acceleration in a laminar, collisionless regime [43,44], to minimize the impact of wave dynamics such as observed closer to the Sun [35,45,46], and to most accurately capture the effects of the reduced outgassing rate. Solar wind protons and electrons are injected at the upstream and side boundaries of the computational domain following the algorithm implemented by Deca *et al.* [47]. The solar wind protons and electrons are sampled from a (drifting) Maxwellian distribution assuming 64 computational particles per cell per species initially. The number of computational particles injected representing the cometary species is scaled accordingly. An overview of all simulation and plasma parameters is given in Table I. In the remainder of this Letter only time-averaged results are shown, computed by taking the mean output over 10 000 computational cycles (0.45 s) after the simulated system has reached steady state.

The GOL, equivalent to a massless electron equation of motion, provides a useful approximation of the electric field, \mathbf{E} , in the plasma frame of reference (here the comet frame) in terms of the magnetic field, \mathbf{B} , the ion mean velocity, \mathbf{u}_i , the

TABLE I. Overview of the plasma parameters and setup of the computational domain. The subscripts “ e , sw ” and “ e , c ” represent solar wind and cometary electron quantities, respectively, and “ p , sw ” and “ p , c ” represent solar wind proton and cometary ion quantities, respectively. $\omega_{pl,e}$ is the upstream electron plasma frequency.

Plasma parameters			
$T_{e,sw}$ [eV]	10	$n_{e,sw}$ [cm^{-3}]	1
$T_{p,sw}$ [eV]	7	$n_{p,sw}$ [cm^{-3}]	1
$T_{e,c}$ [eV]	10	v_{sw} [km s^{-1}]	400
$T_{p,c}$ [eV]	0.026	$\omega_{pl,e}$ [rad s^{-1}]	13165
$m_{p,sw}/m_{e,sw}$	100	B_{IMF} [nT]	6
$m_{p,c}/m_{p,sw}$	20	Q [s^{-1}]	10^{25}
Simulation setup			
Domain size [km^3]	$3200 \times 2200 \times 2200$		
Resolution [km^3]	$10 \times 10 \times 10$		
Time step	4.5×10^{-5}		

current density, \mathbf{j} , the plasma total number density, n , defined as the sum of the solar wind and cometary densities, $n = n_{sw} + n_c$, and the electron pressure tensor, $\mathbf{\Pi}_e$, derived from the electron momentum equation [2]:

$$\mathbf{E} = -(\mathbf{u}_i \times \mathbf{B}) + \frac{1}{en}(\mathbf{j} \times \mathbf{B}) - \frac{1}{en}\nabla \cdot \mathbf{\Pi}_e, \quad (1)$$

where e is the electron electric charge. Its limit of validity assumes (1) typical spatial scales, λ , much larger than the electron inertial length, d_e , and the electron Debye length, $\lambda_{D,e}$, such that quasineutrality is satisfied ($\lambda \gg \lambda_{D,e}, d_e$), and (2) typical frequencies, ω , much smaller than the electron plasma frequency, $\omega_{pl,e}$, and the electron gyrofrequency, $\omega_{cy,e}$, ($\omega \ll \omega_{cy,e} \ll \omega_{pl,e}$). The electric field is then composed of the convective electric field (associated with the ion motion, \mathbf{u}_i), the Hall electric field (associated with the ion-electron dynamical decoupling), and the ambipolar electric field (providing the main contribution to the parallel electric field), respectively. The contribution to the electric field that is associated with the electron inertia is omitted here, but included in the discussion below. In addition, the GOL [Eq. (1)] is formally modified due to mass loading. The contribution of the latter, however, is negligible in the cometary environment simulated here. To compute Eq. (1) we make use of the macroparticle positions, charges, and velocities to obtain the moments (density, mean velocity, and the nine pressure tensor components) for each species. After ensuring that charge neutrality is maintained (accounting for both solar wind and cometary plasma), we derive the total ion velocity, the total charge current and the total electron pressure tensor to retrieve the different terms that would appear in a GOL.

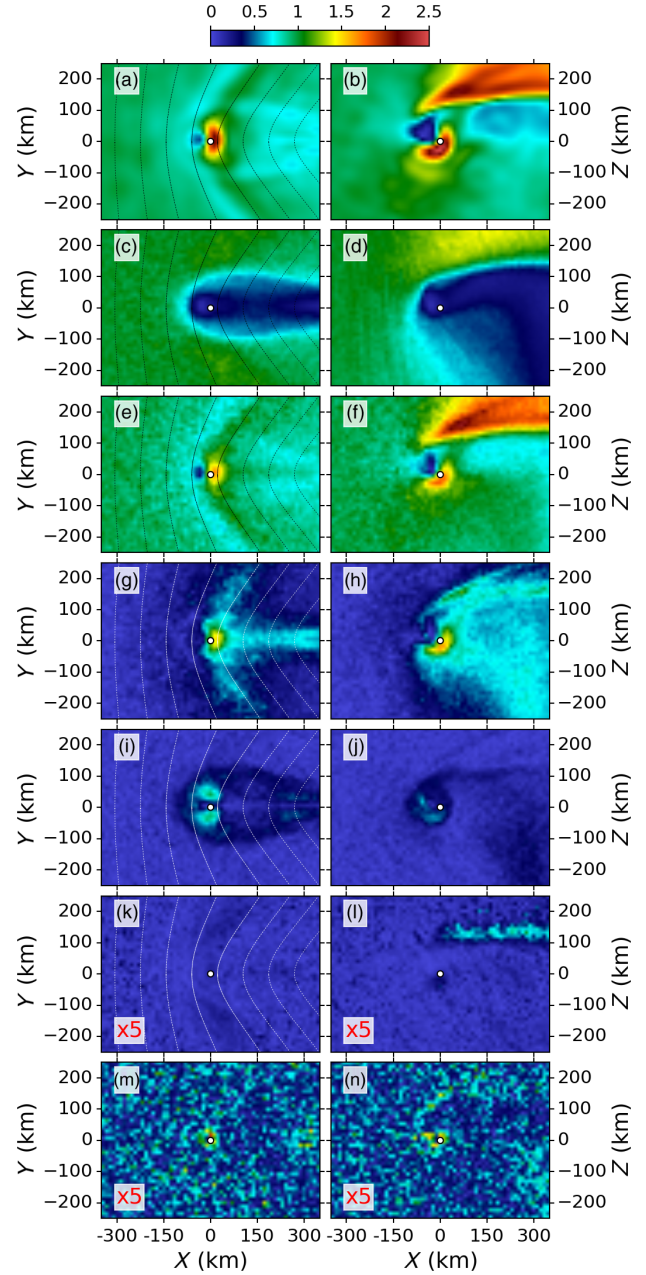


FIG. 2. 2D profiles of electric fields, normalized to $\mathbf{v}_{sw} \times \mathbf{B}_{IMF} = 2.4$ mV/m, along the plane through the cometary nucleus and the direction parallel (left panels) and perpendicular (right panels) to the upstream interplanetary magnetic field. (a,b) Total electric field; (c), (d) ion convective electric field; (e), (f) electron convective electric field; (g), (h) Hall electric field; (i), (j) ambipolar electric field; (k), (l) electron inertial term; (m), (n) residual field. Note, the colors in panels (k), (l), (m), and (n) are scaled by a factor of 5 with respect to the other panels. The coordinate system is cometocentric with the $+x$ direction along the solar wind flow and the $+y$ direction along the interplanetary magnetic field. With exception of panel m, the left-hand panels include also field lines representative of the magnetic topology.

The magnitudes of the different terms of Eq. (1) are shown in Fig. 2 along the plane containing the cometary nucleus and the direction parallel (left column) and perpendicular (right column) to the upstream interplanetary magnetic field. Also included in the figure are the convective electric field generated by the solar wind and cometary electron species combined, and the residual after subtracting the contributions from the electron inertia and all right-hand side terms of Eq. (1) from the total simulated electric field. Upstream and away from the interaction region, the total electric field [Figs. 2(a) and 2(b)] is dominated by the convective term generated by the motion of the solar wind protons and the cometary water ions in the comet frame [Figs. 2(c) and 2(d)]. Closer to the cometary nucleus the situation becomes more complex. As the solar wind plasma becomes more and more mass loaded by cold cometary ions and the solar wind protons are deflected perpendicular to the magnetic field and away from the cometary nucleus [7,48], the ions decouple from the magnetic field while the electrons remain frozen in [Figs. 2(e) and 2(f)]. The dark red shading in the upper right corner of Fig. 2(f) corresponds to the region where the cometary electrons are picked up (see also Fig. 1), creating an electron current that induces the magnetic field pileup upstream of the cometary nucleus [14]. The difference between the ion and electron convective electric fields is the Hall electric field [Figs. 2(g) and 2(h)].

Two more significant regions are noticeable in the total electric field: (1) an area where the electric field magnitude strongly drops, corresponding to the location upstream of the nucleus where the solar wind electrons couple most effectively with the cometary ions, and (2) a banana-shaped region just downstream of the cometary nucleus where the Hall electric field is most pronounced, serving to redirect the solar wind electrons into following the cometary ions through their pickup process. Both regions are most clearly seen in Fig. 2(b).

In the regions where the electron pressure gradient dominates a strong ambipolar electric field is present, e.g., near the outgassing cometary nucleus [43,44,49]. Here the electric field can do work and accelerate electrons parallel to the magnetic field towards the comet [Figs. 2(i) and 2(j)]. Hence, providing further evidence that the ambipolar electric field generates the suprathermal electron population close to the comet [7,43,44]. Note that the analysis presented here cannot exclude an extra electron acceleration source through lower-hybrid waves [50]. In addition, in the perpendicular direction [Fig. 2(j)], a symmetric structure is not expected because of the near-comet cross-field acceleration, i.e., the beginning of the pickup process.

We find that the role of the electron inertia in the time-averaged electric field [$(m_e/e)\nabla \cdot (\mathbf{u}_e \mathbf{u}_e)$, neglected in Eq. (1)] has a negligible contribution in the balance of the total electric field close to the cometary nucleus

[Fig. 2(k)]. On the other hand, it may play a limited role at the inner edge of the region where the solar wind ions are deflected [Fig. 2(l)]. Splitting up the pressure tensor in its diagonal and nondiagonal components (not shown here), the nondiagonal contribution to the electron pressure tensor (i.e., the electron gyroviscosity, typically described by an artificial viscous term in electron fluid models) is entirely localized downstream of the comet and bound to the XZ plane perpendicular to the magnetic field. This narrow area corresponds to the region of space characterized by strong electron velocity shears.

Finally, when evaluating the residual electric field, no structures above the simulation noise level are present [Figs. 2(m) and 2(n)], confirming that the assumptions made to derive the GOL are valid at the comet, at least at the assumed spatial and frequency scales. Note that in case a realistic ion-electron mass ratio is adopted, the residual component would be even smaller. Hence, the observed (already negligible) contribution can be considered an upper limit. The GOL constructed here describes well the physical processes and the electron dynamics at play in the solar wind interaction with a weakly outgassing comet at steady state. Note that the further away from the cometary nucleus, and hence from the region where electron kinetics dominates, the better the classic GOL approximation becomes. This justifies, as expected, the use of reduced models for large scale descriptions.

Now that the validity of the GOL [Eq. (1)] has been verified using self-consistent fully kinetic simulations, we concentrate on the only remaining term that carries information on the electron kinetic evolution through the properties of the electron pressure tensor, namely the ambipolar electric field. In particular, we look for a simple equivalent polytropic closure in the cometary environment that could mimic the mixed cometary and solar wind electron behavior (Fig. 3). We find that the cometary electrons exhibit an apparent isotropic and almost isothermal behavior. The latter is a signature of the steady-state ionization of the expanding cometary ionosphere that creates charged particles characterized by the same initial averaged energy (assumed in the model). The solar wind electrons, on the other hand, exhibit an anisotropic and apparent polytropic behavior. The perpendicular polytropic index measures $\gamma_{e,\perp} \simeq 1.27$, while the parallel polytropic index reveals a knee close to the value of the upstream solar wind density ($n \simeq 1 \text{ km s}^{-1}$), where $\gamma_{e,\parallel} \simeq 1.2$ (respectively 1.62) at lower (respectively higher) densities, implying an electron pressure anisotropy. Note that to have different adiabatic indexes between parallel and perpendicular pressures implies the generation of pressure anisotropies through compression or depression, which are themselves a source of free energy for plasma instabilities to develop. The deviation from polytropic behavior concentrates in the inner coma region (cometary ionosphere). It can be well described by a double adiabatic compression [3] of the

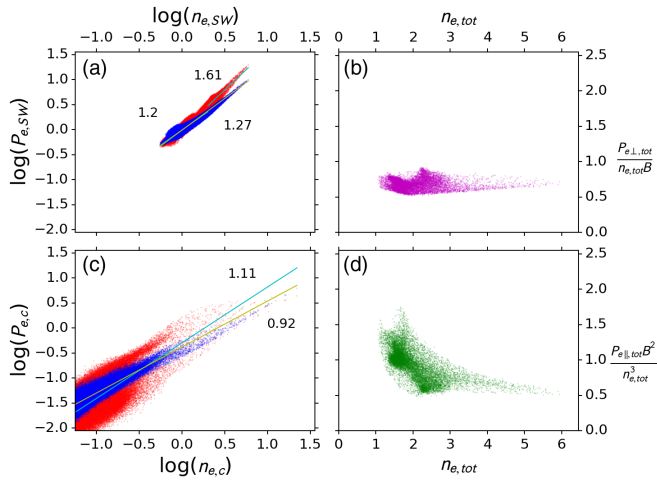


FIG. 3. Electron pressures in the near-cometary environment as a function of the electron number density for (a) the solar wind and (c) the cometary electrons. (b), (d) The adiabatic invariants calculated in a 50 km radius around the nucleus [3] as a function of the electron number density. Note that this radius has been selected empirically in order to most clearly show the influence of the cometary interaction. Each dot in the scatter plots represents one computational cell. The parallel electron pressure is colored red, the perpendicular electron pressure blue. The slope of the best linear fit through the respective population is indicated as well using the complementary color.

perpendicular pressure [Fig. 3(b)]. The parallel electron pressure is not adiabatic [Fig. 3(d)] as a consequence of the parallel electron acceleration in the close plasma environment of a comet [7,49].

The above considerations need to be included for an accurate representation of $\mathbf{\Pi}_e$ when constructing a GOL for a more restrictive computational approach. Figure 4 quantifies the error made [Figs. 4(e) and 4(f)] when characterizing the electron pressure tensor by a single temperature [Figs. 4(c) and 4(d)], here computed using the trace of $\mathbf{\Pi}_e$, or in other words, by neglecting both the off-diagonal and parallel or perpendicular information of the two simulated electron species. Figures 4(a) and 4(b) correspond to Figs. 2(i) and 2(j). Near the nucleus, i.e., in the electron trapping region that is responsible for the generation of the suprathermal electron distributions [7,22,49], Figs. 4(e) and 4(f) reveal differences up to 50% between the full and simplified electron pressure tensor. This is particularly prevalent downstream of the nucleus where the cometary electron pickup process dominates. The correct representation of the ambipolar electric field is crucial for electron acceleration [43,44] and, hence, not doing so might result in a misleading description of the electron dynamics.

Interestingly, Giotto electron and magnetic field measurements from its flyby of comet 1P/Halley [51,52] showed a similar perpendicular polytropic index ($\gamma_{\perp} \sim 1.3$). A significantly smaller value was found, however, for the parallel one ($\gamma_{\parallel} \sim 0.55$), indicative of a more efficient electron cooling mechanism during wave

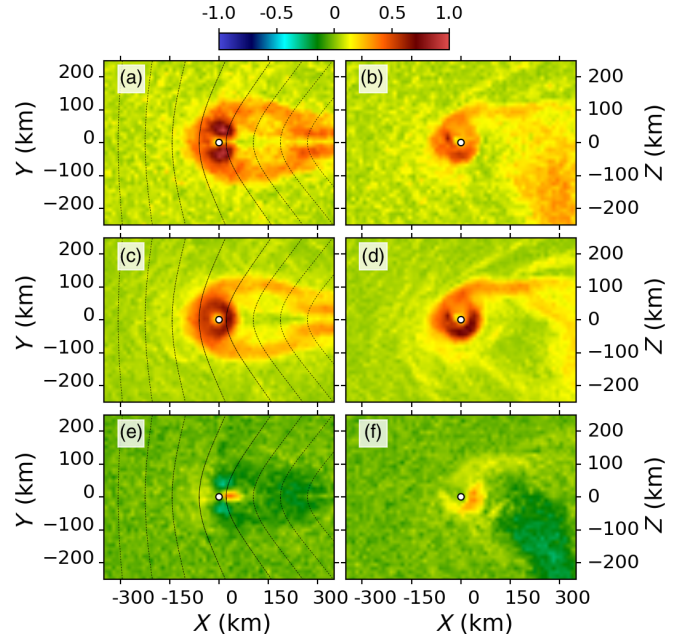


FIG. 4. 2D profiles of the ambipolar electric field, normalized to $\mathbf{v}_{sw} \times \mathbf{B}_{IMF} = 2.4$ mV/m, along the plane through the cometary nucleus and the direction parallel (left panels) and perpendicular (right panels) to the upstream interplanetary magnetic field. (a), (b) Ambipolar electric field computed using the total electron pressure tensor, corresponding to Figs. 2(i) and 2(j); (c), (d) ambipolar electric field computed using the trace of the total electron pressure tensor; (e), (f) difference between the panels above [(c) minus (a), (d) minus (b)]. The coordinate system is cometocentric with the $+x$ direction along the solar wind flow and the $+y$ direction along the interplanetary magnetic field. The left-hand panels include also field lines representative of the magnetic topology.

compression. Note that these observations correspond to suprathermal electrons with energies ranging from 30 to 80 eV, while the mean solar wind and cometary electron energy measured approximately 10 eV.

To conclude, in this Letter, we have simulated the solar wind interaction with a weakly outgassing comet and computed the terms of a GOL directly from the complete electron dynamics of the simulation. The relative importance of each of these terms has allowed us to isolate the driving physics in the various regions of the cometary plasma environment, rather than assuming it. We find that close to the outgassing nucleus the electron pressure gradient dominates, and that at subion scales the total electric field is a superposition of the solar wind convective electric field and the ambipolar electric field. The contributions to the electric field from the electron inertia and mass loading of the solar wind are both negligible. Most importantly, we have shown for a weakly outgassing object that a GOL and the associated electron equation of motion can be applied as long as the full electron pressure tensor is considered to describe the complex electron dynamics of a multispecies plasma environment.

The comparison of our simulations with the limitation of a GOL approximation and the derived polytropic indices deliver compelling information for a wide range of modeling approaches where a self-consistent treatment of the electron dynamics is unfeasible. By averaging the simulation output over time, we have effectively removed wave dynamics and, hence, the polytropic indices deduced here provide an effective electron closure at low frequencies.

This work was supported in part by NASAs Solar System Exploration Research Virtual Institute (SSERVI): Institute for Modeling Plasmas, Atmosphere, and Cosmic Dust (IMPACT), and the NASA High-End Computing (HEC) Program through the NASA Advanced Supercomputing (NAS) Division at Ames Research Center. We acknowledge PRACE for awarding us access to Curie at GENCI@CEA, France. Test simulations were performed at the Lomonosov supercomputing facility (Moscow State University) under Projects No. 1576 and No. 1658. Part of this work was inspired by discussions within International Team 402: Plasma Environment of Comet 67P after Rosetta at the International Space Science Institute, Bern, Switzerland. Work at LPC2E/CNRS was supported by CNES and by ANR under the financial agreement ANR-15-CE31-0009-01. Partial support is also acknowledged by Contract No. JPL-1502225 at the University of Colorado from Rosetta, which is an European Space Agency (ESA) mission with contributions from its member states and NASA. Work at Imperial College London is supported by STFC of UK under Grant No. ST/N000692/1 and ESA under Contract No. 4000119035/16/ES/JD. J. D. gratefully acknowledge support from NASA's Rosetta Data Analysis Program, Grant No. 80NSSC19K1305.

*jandeca@gmail.com

- [1] S. A. Ledvina, Y.-J. Ma, and E. Kallio, *Space Sci. Rev.* **139**, 143 (2008).
- [2] F. Valentini, P. Trávníček, F. Califano, P. Hellinger, and A. Mangeney, *J. Comput. Phys.* **225**, 753 (2007).
- [3] G. F. Chew, M. L. Goldberger, and F. E. Low, *Proc. R. Soc. A* **236**, 112 (1956).
- [4] T. Chust and G. Belmont, *Phys. Plasmas* **13**, 012506 (2006).
- [5] K. Szegő *et al.*, *Space Sci. Rev.* **94**, 429 (2000).
- [6] T. I. Gombosi, in *Magnetotails in the Solar System*, Geophysical Monograph Series Vol. 207, edited by A. Keiling, C. M. Jackman, and P. A. Delamere (2015), pp. 169–188, <https://agupubs.onlinelibrary.wiley.com/doi/10.1002/9781118842324.ch10>.
- [7] J. Deca, A. Divin, P. Henri, A. Eriksson, S. Markidis, V. Olshevsky, and M. Horányi, *Phys. Rev. Lett.* **118**, 205101 (2017).
- [8] K.-H. Glassmeier, H. Boehnhardt, D. Koschny, E. Kührt, and I. Richter, *Space Sci. Rev.* **128**, 1 (2007).
- [9] M. G. G. T. Taylor, N. Altobelli, B. J. Buratti, and M. Choukroun, *Philos. Trans. R. Soc., A* **375**, 20160262 (2017).
- [10] G. Clark, T. W. Broiles, J. L. Burch, G. A. Collinson, T. Cravens, R. A. Frahm, J. Goldstein, R. Goldstein, K. Mandt, P. Mokashi, M. Samara, and C. J. Pollock, *Astron. Astrophys.* **583**, A24 (2015).
- [11] L. Yang, J. J. P. Paulsson, C. S. Wedlund, E. Odelstad, N. J. T. Edberg, C. Koenders, A. I. Eriksson, and W. J. Miloch, *Mon. Not. R. Astron. Soc.* **462**, S33 (2016).
- [12] M. R. Combi and P. D. Feldman, *Icarus* **105**, 557 (1993).
- [13] C. Snodgrass, C. Tubiana, D. M. Bramich, K. Meech, H. Boehnhardt, and L. Barrera, *Astron. Astrophys.* **557**, A33 (2013).
- [14] H. Nilsson, G. S. Wieser, E. Behar, C. S. Wedlund, E. Kallio, H. Gunell, N. J. T. Edberg, A. I. Eriksson, M. Yamauchi, C. Koenders *et al.*, *Astron. Astrophys.* **583**, A20 (2015).
- [15] C. S. Wedlund, E. Kallio, M. Alho, H. Nilsson, G. S. Wieser, H. Gunell, E. Behar, J. Pusa, and G. Gronoff, *Astron. Astrophys.* **587**, A154 (2016).
- [16] C. S. Wedlund, M. Alho, G. Gronoff, E. Kallio, H. Gunell, H. Nilsson, J. Lindkvist, E. Behar, G. S. Wieser, and W. J. Miloch, *Astron. Astrophys.* **604**, A73 (2017).
- [17] C. Simon Wedlund, E. Behar, H. Nilsson, M. Alho, E. Kallio, H. Gunell, D. Bodewits, K. Heritier, M. Galand, A. Beth *et al.*, *Astron. Astrophys.*, <https://doi.org/10.1051/0004-6361/201834881>.
- [18] K. Heritier, M. Galand, P. Henri, F. Johansson, A. Beth, A. Eriksson, X. Vallières, K. Altwegg, J. Burch, C. Carr *et al.*, *Astron. Astrophys.* **618**, A77 (2018).
- [19] N. J. T. Edberg *et al.*, *Geophys. Res. Lett.* **42**, 4263 (2015).
- [20] K. Heritier, P. Henri, X. Vallières, M. Galand, E. Odelstad, A. Eriksson, F. Johansson, K. Altwegg, E. Behar, A. Beth *et al.*, *Mon. Not. R. Astron. Soc.* **469**, S118 (2017).
- [21] H. Nilsson, G. S. Wieser, E. Behar, H. Gunell, M. Wieser, M. Galand, C. Simon Wedlund, M. Alho, C. Goetz, M. Yamauchi, P. Henri, E. Odelstad, and E. Vigren, *Mon. Not. R. Astron. Soc.* **469**, S252 (2017).
- [22] A. I. Eriksson *et al.*, *Astron. Astrophys.* **605**, A15 (2017).
- [23] L. Berčič, E. Behar, H. Nilsson, G. Nicolaou, G. S. Wieser, M. Wieser, and C. Goetz, *Astron. Astrophys.* **613**, A57 (2018).
- [24] Y. D. Jia, M. R. Combi, K. C. Hansen, T. I. Gombosi, F. J. Crary, and D. T. Young, *Icarus* **196**, 249 (2008).
- [25] M. Rubin, C. Koenders, K. Altwegg, M. R. Combi, K.-H. Glassmeier, T. I. Gombosi, K. C. Hansen, U. Motschmann, I. Richter, V. M. Tenishev, and G. Tóth, *Icarus* **242**, 38 (2014).
- [26] M. Rubin, M. R. Combi, L. K. S. Daldorff, T. I. Gombosi, K. C. Hansen, Y. Shou, V. M. Tenishev, G. Tóth, B. van der Holst, and K. Altwegg, *Astrophys. J.* **781**, 86 (2014).
- [27] M. Rubin, T. I. Gombosi, K. C. Hansen, W.-H. Ip, M. D. Kartalev, C. Koenders, and G. Tóth, *Earth Moon Planets* **116**, 141 (2015).
- [28] Z. Huang, G. Tóth, T. I. Gombosi, X. Jia, M. Rubin, N. Fougere, V. Tenishev, M. R. Combi, A. Bieler, K. C. Hansen, Y. Shou, and K. Altwegg, *J. Geophys. Res. (Space Phys.)* **121**, 4247 (2016).
- [29] Y. Shou, M. Combi, G. Toth, V. Tenishev, N. Fougere, X. Jia, M. Rubin, Z. Huang, K. Hansen, T. Gombosi, and A. Bieler, *Astrophys. J.* **833**, 160 (2016).
- [30] N. Gortsas, U. Motschmann, E. Kührt, J. Knollenberg, S. Simon, and A. Boesswetter, *Ann. Geophys.* **27**, 1555 (2009).
- [31] S. Wiehle, U. Motschmann, N. Gortsas, K.-H. Glassmeier, J. Müller, and C. Koenders, *Adv. Space Res.* **48**, 1108 (2011).

- [32] C. Koenders, K.-H. Glassmeier, I. Richter, U. Motschmann, and M. Rubin, *Planet. Space Sci.* **87**, 85 (2013).
- [33] C. Koenders, K.-H. Glassmeier, I. Richter, H. Ranocha, and U. Motschmann, *Planet. Space Sci.* **105**, 101 (2015).
- [34] E. Behar, J. Lindkvist, H. Nilsson, M. Holmström, G. Stenberg-Wieser, R. Ramstad, and C. Götz, *Astron. Astrophys.* **596**, A42 (2016).
- [35] C. Koenders, C. Goetz, I. Richter, U. Motschmann, and K.-H. Glassmeier, *Mon. Not. R. Astron. Soc.* **462**, S235 (2016).
- [36] C. Koenders, C. Perschke, C. Goetz, I. Richter, U. Motschmann, and K. H. Glassmeier, *Astron. Astrophys.* **594**, A66 (2016).
- [37] J. Lindkvist, M. Hamrin, H. Gunell, H. Nilsson, C. Simon Wedlund, E. Kallio, I. Mann, T. Pitkänen, and T. Karlsson, *Astron. Astrophys.* **616**, 10 (2018).
- [38] S. Markidis, G. Lapenta, and Rizwan-uddin, *Math. Comput. Simul.* **80**, 1509 (2010).
- [39] R. J. Mason, *J. Comput. Phys.* **41**, 233 (1981).
- [40] J. U. Brackbill and D. W. Forslund, *J. Comput. Phys.* **46**, 271 (1982).
- [41] G. Lapenta, J. U. Brackbill, and P. Ricci, *Phys. Plasmas* **13**, 055904 (2006).
- [42] K. C. Hansen, K. Altwegg, J.-J. Berthelier, A. Bieler, N. Biver, D. Bockelée-Morvan, U. Calmonte, F. Capaccioni, M. Combi, J. De Keyser *et al.*, *Mon. Not. R. Astron. Soc.* **462**, S491 (2016).
- [43] A. Divin, J. Deca, A. Eriksson, P. Henri, G. Lapenta, V. Olshevsky, and S. Markidis, *Geophys. Res. Lett.* (to be published).
- [44] C. Sishtla, A. Divin, J. Deca, V. Olshevsky, and S. Markidis, *Phys. Plasmas* (to be published).
- [45] I. Richter *et al.*, *Ann. Geophys.* **33**, 1031 (2015).
- [46] T. Karlsson, A. I. Eriksson, E. Odelstad, M. André, G. Dickeli, A. Kullen, P.-A. Lindqvist, H. Nilsson, and I. Richter, *Geophys. Res. Lett.* **44**, 1641 (2017).
- [47] J. Deca, A. Divin, B. Lembège, M. Horányi, S. Markidis, and G. Lapenta, *J. Geophys. Res.* **120**, 6443 (2015).
- [48] E. Behar, B. Tabone, M. Saillenfest, P. Henri, J. Deca, M. Holmström, and H. Nilsson, *Astron. Astrophys.* **620**, A35 (2018).
- [49] H. Madanian, T. E. Cravens, A. Rahmati, R. Goldstein, J. Burch, A. I. Eriksson, N. J. T. Edberg, P. Henri, K. Mandt, G. Clark, M. Rubin, T. Broiles, and N. L. Reedy, *J. Geophys. Res. (Space Phys.)* **121**, 5815 (2016).
- [50] T. W. Broiles, J. L. Burch, K. Chae, G. Clark, T. E. Cravens, A. Eriksson, S. A. Fuselier, R. A. Frahm, S. Gasc, R. Goldstein, P. Henri, C. Koenders, G. Livadiotis, K. E. Mandt, P. Mokashi, Z. Nemeth, E. Odelstad, M. Rubin, and M. Samara, *Mon. Not. R. Astron. Soc.* **462**, S312 (2016).
- [51] G. Belmont and C. Mazelle, *J. Geophys. Res.* **97**, 8327 (1992).
- [52] C. Mazelle and G. Belmont, *Geophys. Res. Lett.* **20**, 157 (1993).